Novel Hybrid Modulation Schemes Extending the Reactive Power Control Range of Conventional and Sparse Matrix Converters Operating at Maximum Output Voltage

Frank Schafmeister and Johann W. Kolar

ETH Zurich, Power Electronic Systems Laboratory
ETH Zentrum / ETL H17, Physikstr. 3, CH-8092 Zurich / SWITZERLAND
Tel.: +41-1-632 2833   Fax.: +41-1-632 1212
email: sekretariat@lem.ee.ethz.ch

Abstract. *Two novel modulation schemes are proposed for three-phase AC-AC Sparse Matrix Converters (SMC) which facilitate the formation of reactive input current for purely reactive load or purely active load and operation at the modulation limit. The derivation of the modulation schemes which also could be employed for Conventional Matrix Converters and rely on a decoupling of the output voltage and the input current formation is described in detail. Furthermore, the operating limits, i.e. the maximum reactive input current which could be formed for given modulation index and load current amplitude are determined. Finally, all theoretical considerations are verified by digital simulations of a 7.5kW Very Sparse Matrix Converter.*

I. INTRODUCTION

Sparse Matrix Converters (SMC, [1], cf. **Fig.1**) are functionally equivalent to Conventional Matrix Converters (CMC) but are characterized by a lower realization effort and a lower control complexity and are therefore especially interesting for an industrial application.
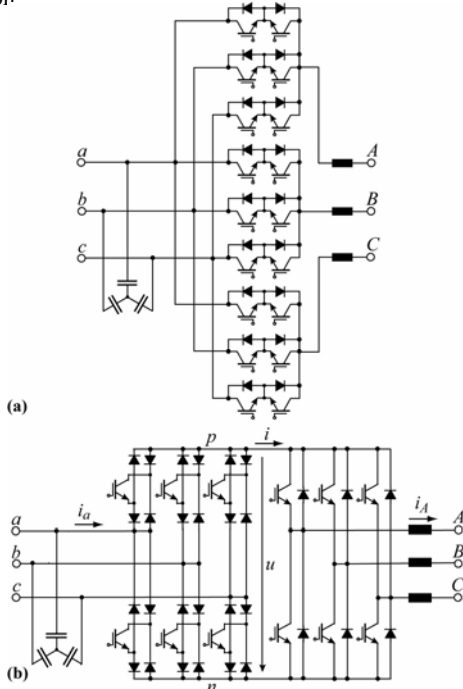

Fig.1: Topology of the Conventional Matrix Converter (CMC, **(a)**) and of the Very Sparse Matrix Converter (VSMC, **(b)**) according to [1].

By proper control of the input stage within each pulse half period two line-to-line voltages are switched into the DC link of the SMC. There, the input stage commutation is at zero current (cf. *i* in Fig.6 in [1], [2]) what allows to avoid a multi-step commutation scheme which has to be performed in dependency on the sign of the commutating voltage or direction of the commutating current for the CMC and results in low switching losses and high converter reliability.

For conventional modulation of a SMC (being equivalent to indirect or virtual DC link modulation of a CMC), we have for the relative turn-on times of the single switching states [1-3] e.g. for φ_1 in $-\pi/6$ …$+\pi/6$ and φ_2 in $0…+\pi/3$ (as given in Fig.2)

$$d_{ab} = cos(\varphi_1 + \pi/3)$$
$$d_{ac} = cos(\varphi_1 - \pi/3)$$
$$\delta_{(100)} = M_{12} \cdot cos(\varphi_2 + \pi/6)$$
$$\delta_{(110)} = M_{12} \cdot sin(\varphi_2)$$
(1)

$$\delta_{(100),ac} = d_{ac} \cdot \delta_{(100)}$$
$$\delta_{(110),ac} = d_{ac} \cdot \delta_{(110)}$$
$$\delta_{(110),ab} = d_{ab} \cdot \delta_{(110)}$$
$$\delta_{(100),ab} = d_{ab} \cdot \delta_{(100)}$$
(2)

with

$$M_{12} := \frac{2}{\sqrt{3}} \frac{\hat{U}_2}{\hat{U}_1}$$
(3)

There, the operating range is defined by [1], [5]

$$\hat{U}_2 = \frac{\sqrt{3}}{2} M_{12}\hat{U}_1 \cdot cos(\Phi_1)$$
(4)

$$\hat{I}_1 = \frac{\sqrt{3}}{2} M_{12}\hat{I}_2 \cdot cos(\Phi_2).$$
(5)

Accordingly, for conventional modulation no output voltage fundamental could be formed for operation with $\Phi_1 = \pm\pi/2$ (cf. (4)), or in case of $\Phi_2 = \pm\pi/2$, no load current could be transferred to the input for generating a (reactive) input current fundamental ($i_{1q}=0$, cf. (5)).

Novel hybrid modulation schemes facilitating a utilization of a purely reactive load current $i_2 = \pm j.i_{2q}$ of a SMC for the formation of reactive input current have been proposed recently by the authors in [3]. For employing such modulation schemes, which rely on a decoupling of the output voltage and the input current formation, e.g. the reactive current of an asynchronous machine supplied by the SMC could be used for the compensation of the reactive input filter capacitor current also for no load operation.

However, so far no modulation scheme has been described which would allow the formation of a reactive input current component at full output voltage while supplying a purely active load, i.e.

$$\hat{U}_2 = \frac{\sqrt{3}}{2}\hat{U}_1 \wedge \Phi_2 = 0 \Rightarrow \Phi_1 = 0$$

seems to be a basic operating limit of the SMC or CMC [4].

In this paper, first the hybrid modulation schemes introduced in [3] are briefly discussed in **Section 2.A** (*Two-Vector-Scheme*) and **Section 2.B** (*Three-Vector-Scheme*). Based on this an optimum combination of the *Two- and Three-Vector-Scheme* is proposed (cf. **Section 2.C**) which allows an extension of the operating limit, i.e. a maximum increase of the amplitude limit of the reactive input current in the upper modulation range. In **Section 3** the modulation

schemes are adapted for operation at $\Phi_2 = 0$ and it is shown that a reactive input current component could be formed even at full output voltage. **Section 3.A** is dedicated to the analysis of the adapted Two-Vector-Scheme for purely active load and **Section 3.B** describes the Three-Vector-Scheme for purely active load. The optimum combination of both schemes concerning the operating range is treated in **Section 3.C.** Finally, the proposed modulation schemes are verified by digital simulations in **Section 4**.

II. REACTIVE INPUT CURRENT FORMATION FOR PURELY REACTIVE LOAD ($\Phi_1 = \pm \pi/2$, $\Phi_2 = \pi/2$)

A. Two-Vector Modulation Scheme for Purely Reactive Load

The space vector diagrams describing the *Two-Vector Modulation Scheme* [3] are depicted in **Fig. 2**.
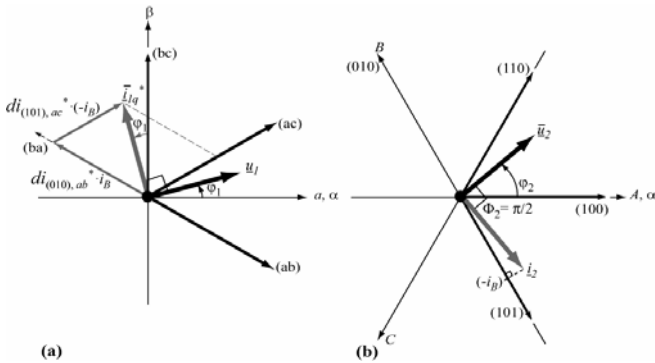

Fig.2: Space vector diagrams of the SMC input stage **(a)** and output stage **(b)** for purely reactive input and output power. The formation of the local average value $\underline{i}_{1q}{}^*$ of the reactive input current using the vectors *(ba)* and *(ac)* shown in **(a)** characterizes the *„Two-Vector Scheme"*.

As explained in detail in [3], the analysis of the geometrical relations of Fig.2 directly yields the relative turn-on times

$$di_{(010),ab}{}^* = \frac{2}{\sqrt{3}} MI \cdot \frac{\cos(\varphi_1 - \pi/6)}{\cos(\varphi_2 - \pi/6)}$$

$$di_{(101),ac}{}^* = \frac{2}{\sqrt{3}} MI \cdot \frac{\cos(\varphi_1 + \pi/6)}{\cos(\varphi_2 - \pi/6)} \qquad (6)$$

Which have to be set for the formation of a reactive input current characterized by the current transfer ratio

$$MI := \frac{\hat{I}_{1q}{}^*}{\hat{I}_2} \qquad . \qquad (7)$$

The turn-on times defined by (6) are applied in the second half of a pulse period for the formation of the reactive input current without taking influence on the output voltage which is formed in the first half of a pulse period by conventional modulation. According to this combination of a voltage forming and current forming pulse half period the modulation scheme is denoted as *Hybrid Modulation* in the following. The basic pulse pattern comprising both pulse half periods is shown in Fig.6 in [3].

It has to be pointed out, that for the formation of the reactive input current the output phase current showing the largest instantaneous value is switched into the DC link (first with negative, then with positive polarity, i.e. i_B, $-i_B$ in the case at hand, cf. Fig.2b). The final pulse pattern shown in **Fig.3** merging the DC link current pulses i occurring for the same DC link voltage level u, where the relation $i_A + i_B + i_C = 0$ of the output phase currents is considered and/or the sum of two pulses (two segments of the output phase currents) is expressed by the third phase current level.

We then have for the total (relative) turn-on time $d_{tot,2V}$ of the active switching states of the final pulse pattern depicted in Fig.3
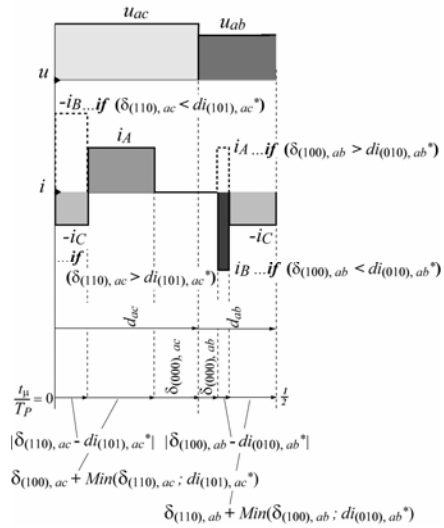

Fig.3: Final pulse pattern resulting for the *„Two-Vector Scheme"* after merging the output voltage and the input reactive current forming halves of the original pulse period (cf. Fig.6 in [3]).

$$d_{tot,2V} =$$
$$= \left| \delta_{(110),ac} - di_{(101),ac}{}^* \right| + \delta_{(100),ac} + Min(\delta_{(110),ac}, di_{(101),ac}{}^*) + \qquad (8)$$
$$+ \left| \delta_{(100),ab} - di_{(010),ab}{}^* \right| + \delta_{(110),ab} + Min(\delta_{(100),ab}, di_{(010),ab}{}^*)$$

Considering (1), (2) and (6) the total turn-on time (8) depends on four variables: φ_1, φ_2, M_{12} and MI where the operating limit is defined by $d_{tot,2V}=1$ (no remaining free-wheeling interval). Restricting the consideration to the critical angles $\varphi_{1,crit}$, $\varphi_{2,crit}$ which are associated with the maximum of $d_{tot,2V}$ and/or to the position within a mains / load period where overmodulation occurs first, (8) finally results in the dependency of MI on M_{12} shown in **Fig.4** characterizing the operating limit. The limit is found by numerical calculations but also could be verified analytically [3]. With reference to (4) it has to be pointed out that the *Two-Vector Scheme* allows the formation of a reactive input current up to $\hat{I}_{1q}=0.12\,\hat{I}_2$ even at full output voltage ($M_{12} = 1$).

The dependency of the critical angle $\varphi_{1,crit,2V}$ on the modulation index M_{12} is depicted in **Fig.5**. Starting from 0, $\varphi_{1,crit,2V}$ increases until $\pi/6$ is reached for $M_{12,Lim,2V}=2/3$. For $M_{12,Lim,2V}>2/3$ the critical angle remains constant at $\pi/6$. For the critical position in the output period we have $\varphi_{2,crit,2V}=0$ independent of M_{12}.
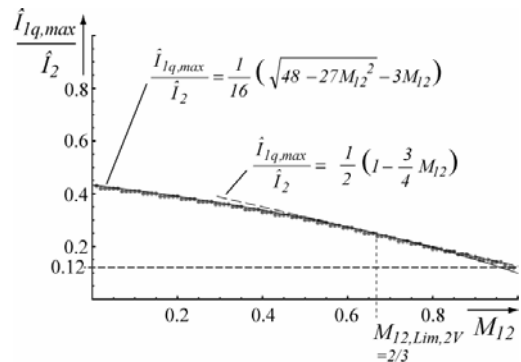

Fig.4: Analytically derived and numerically calculated (dotted line) current transfer limit of the *Two-Vector Scheme*. $M_{12,Lim,2V}$ marks the transition from the current limiting to the voltage limiting operating range and/or from (9) to (12). Even at full output voltage ($M_{12} = 1$) a reactive input current up to $\hat{I}_{1q}=0.12\,\hat{I}_2$ could be formed.

In the following a brief explanation of the physical reasons of the operating limits of the SMC concerning reactive input current formation which are present in similar form for all modulation schemes proposed in this paper shall be given. This directly leads to an analytical description of the operating limits and the critical angles.

- **Current Limited Operating Range ($M_{12} = 0...M_{12,Lim,2V}$)**
  Considering the input stage space vector diagram (cf. Fig.2a), in the case of low output voltage ($M_{12} \approx 0$) the lowest magnitude of the reactive input current $\underline{i}_{1q}$ (local average value over a pulse period) which defines $\hat{I}_{1q}$ can be formed in case the input current reference vector $\underline{i}_{1q}^*$ is aligned with the symmetry axis of the vectors *(ac)* and *(ba)*, and/or for $\varphi_1=0$. Since the magnitude of the current vectors *(ac)* and *(ba)* is defined by the output phase current of largest instantaneous value ($\pm i_B$), the minimum of $\hat{I}_{1q}$ over φ_2 is defined by the minimum of $|\pm i_B|$, i.e. $\varphi_{2,crit,I}=0$ (or $\varphi_2 = \pi/3$) is the critical value (cf. Fig.2b). In consequence, for $M_{12} \approx 0$ the maximum achievable *MI* is defined by $\cos(\pi/3) \cdot \cos(\pi/6) = \tfrac{1}{2}\sqrt{3}/2$.

  For $M_{12} > 0$ the operating limit MI_{max} is further restricted by the finite turn on times of the active switching states of the SMC output stage resulting in DC link current pulses lowering the local reactive input current average value (cf. Fig.3). As MI_{max} still is basically determined by the magnitude of input current space vectors this operating range is denoted as *Current Limited Range*. There, $\varphi_{2,crit,I}$ remains constant, while $\varphi_{1,crit,I}$ increases with increasing M_{12} and reaches $\varphi_{1,crit,II}=\pi/6$ for $M_{12,Lin,2V}=2/3$.

- **Voltage Limited Operating Range ($M_{12} = M_{12,Lim,2V} ...1$)**
  For $M_{12,Lin,2V} >2/3$, $\varphi_{1,crit,II}$ remains at $\pi/6$. This is equivalent to the fact that the output voltage formation is mainly determining MI_{max}. Accordingly, this operating range is denoted as *Voltage Limited Range*. The critical load phase angle $\varphi_{2,crit,II}$ is again constant independent of M_{12}.

  For voltage limited operation the pulse merging for $\varphi_{1,crit,II}$, $\varphi_{2,crit,II}$ does not reduce but increase the total turn-on time. There, within the output voltage forming half of the pulse period only one line-line input voltage is switched into the DC link and only one output phase current is switched into the DC link which shows the same polarity as the current pulse used for the reactive input current formation. This special case is given for $\varphi_1=\varphi_{1,crit,II}=\pi/6$ and $\varphi_2=\varphi_{2,crit,II}=0$ (within the whole output voltage forming half period only $u = u_{ac}$ and $i = i_A$ is applied) and/or for $\varphi_1= -\pi/6$ and $\varphi_2 = \pi/3$ ($u = u_{ab}$, $i = -i_C$).
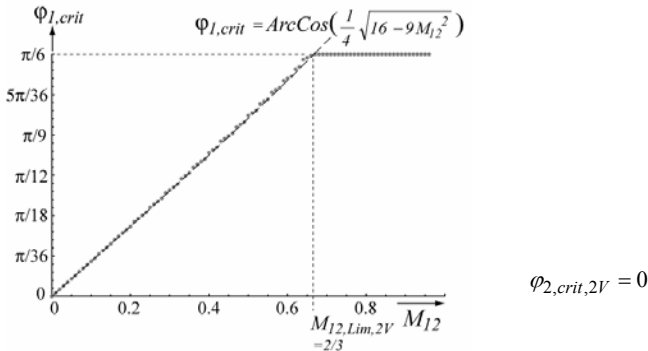

Fig.5: Critical angle $\varphi_{1,crit,2V}$, which represents the position within a mains period where overmodulation concerning reactive input current formation occurs first. The analytical expression (10) for current limited operation ($M_{12} = 0...2/3$) is clearly verified by the numerical results shown by a dotted line. For voltage limited operation ($M_{12} = 2/3...1$) the critical angle remains constant at $\varphi_{1,crit,2V}=\pi/6$; for φ_2 we have $\varphi_{2,crit,2V}=0$ independent of M_{12}.

Based on these considerations analytical expressions defining the operating limits are derived in the following.

As $\varphi_{2,crit,2V} =0$ is given for *Current Limited Operation* one of the four variables of (8) is eliminated. For defining φ_1, the maximum of (8) over φ_1 has to be determined what results in an expression $\varphi_{1,crit} = f(M_{12}, MI)$, cf. (22) in [3]. Inserting $\varphi_{1,crit}$ into (8) and setting $d_{tot,2V}=1$ yields

$$MI_{max,2V,I} = \frac{1}{16}\left(\sqrt{48 - 27M_{12}^2} - 3M_{12}\right). \tag{9}$$

For determining $\varphi_{1,crit} = f(M_{12})$, (9) has to inserted into $\varphi_{1,crit} = f(M_{12}, MI)$ what results in

$$\varphi_{1,crit,2V}(M_{12}) = ArcCos\left[\tfrac{1}{4}\sqrt{16 - 9M_{12}^2}\right] \tag{10}$$

and

$$\varphi_{2,crit,2V} = 0. \tag{11}$$

For *Voltage Limited Operation* we have $\varphi_{1,crit,2V} =\pi/6$, $\varphi_{2,crit,2V} =0$ what directly results in the desired function

$$MI_{max,2V,II} = \frac{1}{2}\left[1 - \tfrac{3}{4}M_{12}\right]. \tag{12}$$

Equating (9) and (12) leads to the modulation index defining the transition between *Current-* and *Voltage Limited Operation*

$$M_{12,Lim,2V} = \frac{2}{3}. \tag{13}$$

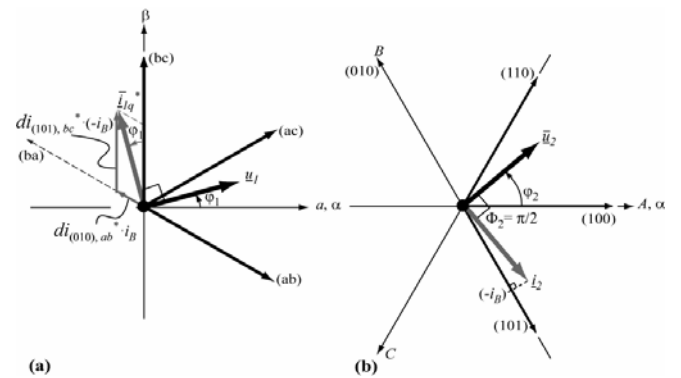### B. Three-Vector Modulation Scheme for Purely Reactive Load

Fig.6: Space vector diagrams of the SMC input stage **(a)** and output stage **(b)** for purely reactive input and output power. The formation of the reactive input current vector $\underline{i}_{1q}^*$ (local average value) using the vectors *(ba)* and *(bc)* as shown in **(a)** characterizes the „*Three-Vector Scheme*" (for the output voltage formation *(ac)* and *(ab)* are employed, so in total 3 different vectors are utilized within each pulse period).

The *Three-Vector Scheme* employs input current space vectors for the current formation which are directly neighboring the desired reactive input current vector $\underline{i}_{1q}^*$ (formed in the average over a pulse period), e.g. *(bc)* and *(ba)* as shown in **Fig.6**a. Accordingly, in contrary to the Two-Vector Scheme, for the *Three-Vector Scheme* the sign of φ_1 has to be considered. Based on the geometrical relations of Fig.6 we have for the additional turn-on times for $\varphi_1 \geq 0$

$$di_{(010),ab}^* = \frac{2}{\sqrt{3}}MI \cdot \frac{\sin(\varphi_1)}{\cos(\varphi_2 - \pi/6)}$$
$$di_{(101),bc}^* = \frac{2}{\sqrt{3}}MI \cdot \frac{\cos(\varphi_1 + \pi/6)}{\cos(\varphi_2 - \pi/6)} \tag{14}$$

Where the negative current pulse i_B has to be assigned to *(ab)*. In analogy for $\varphi_1 < 0$

$$di_{(101),ac}^* = \frac{2}{\sqrt{3}}MI \cdot \frac{\sin(|\varphi_1|)}{\cos(\varphi_2 - \pi/6)}$$
$$di_{(010),cb}^* = \frac{2}{\sqrt{3}}MI \cdot \frac{\cos(|\varphi_1| + \pi/6)}{\cos(\varphi_2 - \pi/6)} \tag{15}$$

is valid where the negative current pulse i_B has to be assigned to *(cb)*.

Applying pulses with turn on times defined by (14), (15) in each second pulse half period (cf. Fig.9 of [3]) and merging the current pulses occurring for the DC link voltage level which is present in pulse half periods (in the case at hand u_{ab}) finally results in the pulse pattern shown in **Fig.7**.
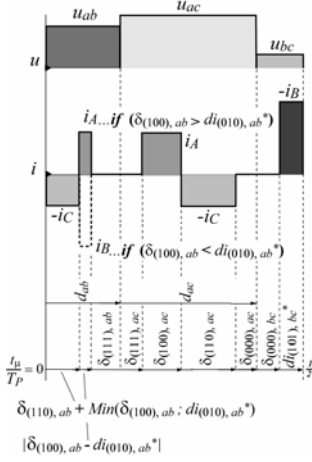
Fig.7: Final pulse pattern resulting for the „Three-Vector Scheme" after merging input current pulses occurring for $u=u_{ab}$ being present in both halves of the original pulse period depicted in Fig.9 of [3].

Fig.9: Dependency of the critical angle values $\varphi_{1,crit,3V}$ **(a)** and $\varphi_{2,crit,3V}$ **(b)** of the *Three-Vector-Scheme* on M_{12}. Changing from the current limited operating range ($M_{12} = 0...0.638$) to the voltage limited range ($M_{12} = 0.638...1$) clearly affects both angle values what identifies a maximum of $d_{tot,3V}$ in the φ_1-φ_2-plane. The analytical expression (20) for $\varphi_{1,crit,3V}$ coincides with the numeric results.

Due to the third DC link voltage level utilized for the reactive input current formation, only two current pulses can be merged. The total turn-on time of the active switching states then results as

$$d_{tot,3V} = \delta_{(110),ab} + Min(\delta_{(100),ab}, di_{(010),ab}{}^*) +$$
$$+ \left| \delta_{(100),ab} - di_{(010),ab}{}^* \right| + \delta_{(100),ac} + \delta_{(110),ac} + di_{(101),bc}{}^* . \quad (16)$$

Numerically evaluating (16) including the foregoing determination of the maxima within the φ_1-φ_2-plane for each M_{12} results in the limit represented by a dotted line in **Fig.8**. Again, the analytically determined transfer limit coincides with the numerical calculation.

Based on the considerations of Section 2.A we receive for the *Current Limited Operating Range*

$$MI_{max,3V,I} = \frac{3}{16}(\sqrt{16 - 3M_{12}{}^2} - 3M_{12}), \quad (17)$$

and for the *Voltage Limited Operating Range*

$$MI_{max,3V,II} = 1 - M_{12} . \quad (18)$$

The transition between the operating ranges is defined by

$$M_{12,Lim,3V} = \frac{2}{19}(14 - 3\sqrt{7}) \approx 0.638 . \quad (19)$$
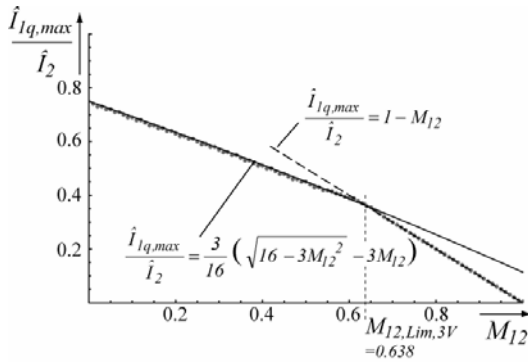

Fig.8: Analytically derived and numerically calculated (dotted line) transfer limits of the *Three-Vector Scheme*. The transition from the current limited to the voltage limited operating range (at $M_{12,Lim,3V}$) takes larger influence on maximum reactive current transfer ration than for the *Two-Vector Scheme*.

The critical position $\varphi_{1,crit,3V}$ is defined for the *Current Limited Operating Range* by

$$\varphi_{1,crit,3V}(M_{12}) = ArcCos\left[\frac{\sqrt{3}}{8}\left(M_{12} + \sqrt{16 - 3M_{12}{}^2}\right)\right] \quad (20)$$
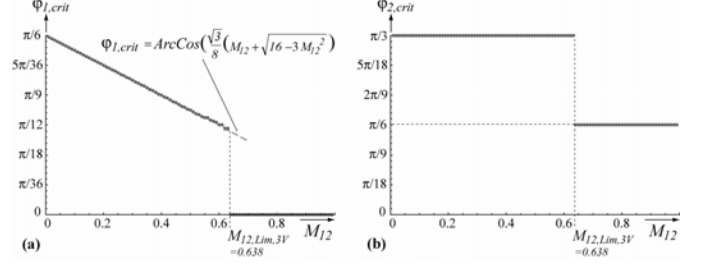
as graphically shown in **Fig.9**a.

- **Current Limited Operating Range** $(M_{12} = 0...M_{12,Lim,3V})$
  Considering the space vector diagram (cf. Fig.6), the operating limit at $M_{12} \approx 0$ again will be given for $\underline{i_{1q}}^*$ located symmetrically in the middle of the current forming vectors *(bc)* and *(ba)*, i.e. for $\varphi_1 = \pi/6$. Furthermore, again $\varphi_2 = \pi/3$ (or $\varphi_2 = 0$) are resulting in a minimum value of $|\pm i_B|$ and/or in a minimum current space vector magnitude. Therefore, for $M_{12} = 0$ the maximum achievable *MI* is defined by $\cos(\pi/6) \cdot \cos(\pi/6) = \frac{3}{4}$.

- **Voltage Limited Operating Range** $(M_{12} = M_{12,Lim3V} ...1)$
  The voltage limiting condition is given for $\varphi_{1,crit} = 0$ and $\varphi_{2,crit} = \pi/6$. In this case no freewheeling interval remains for $M_{12} = 1$ and as a consequence the current forming pulse i_B which would occur for the additional (third) DC link voltage level cannot be applied anymore. Therefore, no reactive input can be formed at full modulation.

C. Optimum Combination of the Two- and Three-Vector Scheme

For Sections 2.A and 2.B the *Two-Vector* or *Three-Vector Scheme* has been applied within the whole mains and load period, i.e. within the whole φ_1-φ_2-plane.
However, as shown in the following, within a certain range of M_{12} advantageously different schemes could be use for defined areas of the φ_1-φ_2-plane.

Aiming for a maximum *MI* the modulation scheme with the lower associated total turn-on time can be denoted as optimal,

$$d_{tot,opt} = \begin{cases} d_{tot,2V} : d_{tot,2V} < d_{tot,3V} \\ d_{tot,3V} : d_{tot,2V} \geq d_{tot,3V} \end{cases} . \quad (21)$$

The evaluation of (21) is graphically shown in **Fig.10** for varying M_{12}. There, dark areas marks are indicating $d_{tot,2V} = d_{tot,3V}$, and therefore the boundaries of the optimum domains of the two schemes. In addition the maxima of $d_{tot,2V}$, $d_{tot,3V}$ and $d_{tot,opt}$ are identified. Starting with $M_{12} = 0.65$ **(a)** the *Three-Vector-Scheme* resides in the *Voltage Limiting Operating Range*. The global application of this scheme is still optimal. But with increasing M_{12} **((b), (c))** the utilization of the *Two-Vector Scheme* in the vicinity of plane center becomes advantageous. Due to the fact that the maximum of $d_{tot,3V}$, which was formerly defining the operating limit, is located at the plane center point ($\varphi_{1,crit,3V}=0$, $\varphi_{2,crit,3V}=\pi/6$) where the *Two-Vector Scheme* provides lower total turn-on times, the operating limit will be extended by using this scheme. This can be seen clearly from **Fig.11**. As can be seen from **(b) - (d)**, in the vicinity of the maximum of the *Three-Vector Scheme* the *Two-Vector-Scheme* showing a lower $d_{tot,2V}$ is applied and vice versa.
When approaching full modulation **(d)**, the domain of the *Three-Vector-Scheme* vanishes and for $M_{12} \approx 1$ the *Two-Vector-Scheme* constitutes the optimum modulation scheme.
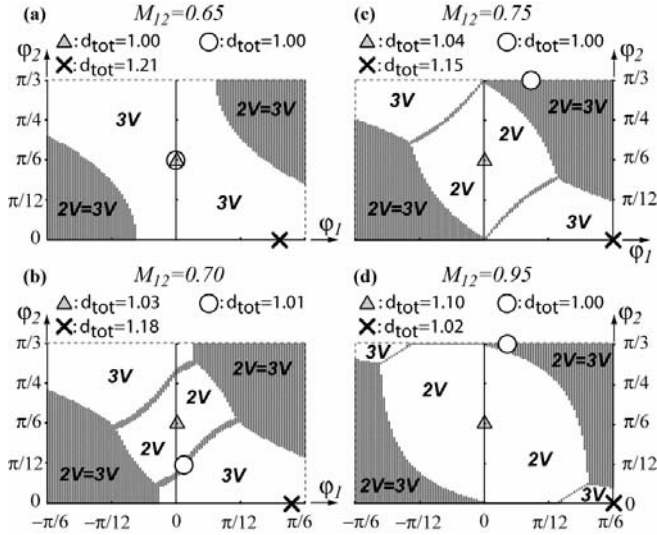
(a) $M_{12}=0.65$
$\triangle: d_{tot}=1.00$ $\bigcirc: d_{tot}=1.00$
$\times: d_{tot}=1.21$

(c) $M_{12}=0.75$
$\triangle: d_{tot}=1.04$ $\bigcirc: d_{tot}=1.00$
$\times: d_{tot}=1.15$

(b) $M_{12}=0.70$
$\triangle: d_{tot}=1.03$ $\bigcirc: d_{tot}=1.01$
$\times: d_{tot}=1.18$

(d) $M_{12}=0.95$
$\triangle: d_{tot}=1.10$ $\bigcirc: d_{tot}=1.00$
$\times: d_{tot}=1.02$

Fig.10: Domains within the φ_1-φ_2-plane defining the optimum application areas of the *Two-Vector* or *Three-Vector Modulation Scheme* with respect to minimum $d_{tot,act}$ (for short denominated as d_{tot} in the following) for different values of M_{12}. The dark color marks areas where $d_{tot,2V} = d_{tot,3V}$ is valid. *Remark:* The maxima of d_{tot} for the *Two-Vector, Three-Vector,* and the *Optimal-Scheme* are occurring symmetrically to the plane center point. For the sake of clarity, the maxima are only marked in the positive φ_1–half plane. *Legend:* $\times$: maximum of $d_{tot,2V}$; $\triangle$: max. of $d_{tot,3V}$; $\bigcirc$: max. of $d_{tot,opt}$.
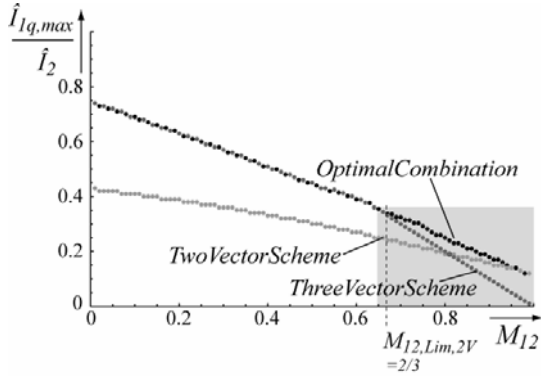
Fig.11: Comparison of the operating limits of the modulation schemes. Up to $M_{12,Lim,2V}$ the *Three-Vector-Scheme* results in the maximum value of *MI*. From there, *MI* can be increased by changing to the *Two-Vector Scheme* within sections of the φ_1-φ_2-plane as shown in Fig.10. For full output voltage ($M_{12}=1$) the *MI* limit is defined by the *Two-Vector Scheme*.
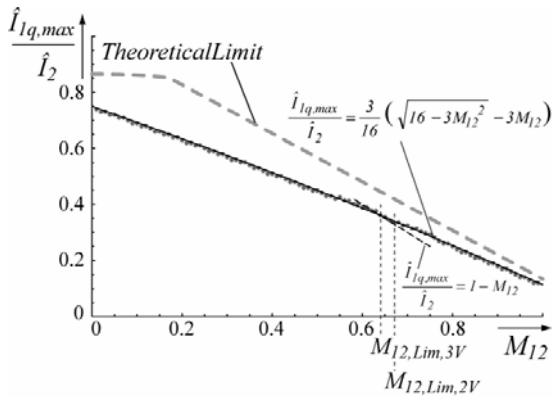
Fig.12: Above $M_{12,Lim,2V}$ numerical analysis proves the maximum reactive current transfer limit achieved by optimum modulation to return to the limit (17) valid for the *Three-Vector-Scheme* in the current limited operating range. Within the small interval between $M_{12,Lim,3V}$ and $M_{12,Lim,2V}$ (18) determines the limit. Furthermore shown is the theoretical limit of reactive current transfer for the CMC according to [4].
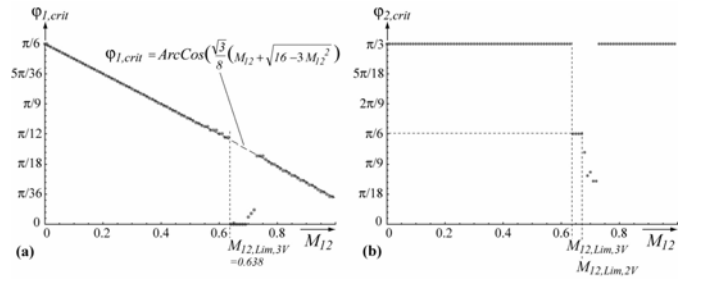
Fig.13: Critical angles $\varphi_{1,crit,opt}$ **(a)** and $\varphi_{2,crit,opt}$ **(b)** of the optimum modulation in dependency on M_{12}. In accordance with Fig.12 and Fig.10a the *Three-Vector-Scheme* voltage limit is reached at $M_{12,Lim,3V}$. For further increasing M_{12}, $M_{12,Lim,2V}$ is reached where again a transition to the critical angle values of the *Three-Vector-Scheme* in current limited operation occurs.

As shown in **Fig.12**, the numerically calculated operating limit of optimum modulation returns above $M_{12,Lim,2V}$ to the limit defined by (17) for the *Three-Vector-Scheme* in current limited operation (cf. also **Fig.13**).

Finally, it should be pointed out, that the implementation of the proposed optimum modulation scheme could be achieved without significantly increasing the realization effort, since all turn-on times have to be calculated for implementing a modulation algorithm. Therefore, only the sums (8) and (16) have to be compared and the modulation scheme showing the lower total turn-on time has to be selected.

III. REACTIVE INPUT CURRENT COMPONENT FORMATION FOR PURELY ACTIVE LOAD ($\Phi_2= 0$) AT FULL OUTPUT VOLTAGE

A. Two-Vector Modulation Scheme for Purely Active Load

For the following considerations the load is assumed to draw a purely active current, i.e. $\Phi_2 =0$. Considering this output phase current displacement, the space vector diagram Fig.2 is still valid.

Contrary to $\Phi_2 =\pm\pi/6$ now the current in output phase ($-C$) shows the largest instantaneous value. Accordingly, in the formulas for the additional turn-on times only the phase shift of φ_2 in the cosine terms of the denominator has to be adapted

$$di_{(001),ab}{}^* = \frac{2}{\sqrt{3}}MI \cdot \frac{\cos(\varphi_1 - \pi/6)}{\cos(\varphi_2)}$$

$$di_{(110),ac}{}^* = \frac{2}{\sqrt{3}}MI \cdot \frac{\cos(\varphi_1 + \pi/6)}{\cos(\varphi_2)} \tag{22}$$

Fig.14 shows a pulse period of the basic hybrid modulation scheme comprising an output voltage/active input active current forming half period and a subsequent half period dedicated to the formation of a reactive input current component. This basic scheme is largely equivalent to the scheme employed for purely reactive load (cf. Fig.6 in [3]). As a main difference here in total only two different output phase currents are switched into the DC link. Therefore, the merging of current pulses results in a partial pulse compensation.

E.g. in Fig.14 the pulse i_C occurring for $u=u_{ab}$ in the second pulse half period overcompensates the neighboring pulse ($-i_C$) of the first half period and reduces the total turn-on time. The second pulse of the reactive current forming interval ($-i_C$) occurring for $u=u_{ac}$ cannot be compensated but has to be added to the pulse ($-i_C$) of the voltage forming interval and therefore increases the total turn-on time. This finally results in the pulse pattern shown in **Fig.15**.
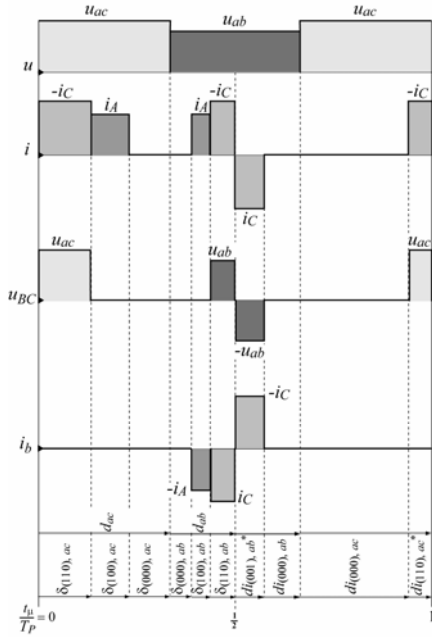
Fig.14: Hybrid modulation for reactive input current formation in case of purely active load. The first half of each pulse period is dedicated to the formation of the output voltage and the active input current component. Subsequently the reactive input current component is formed in the second pulse half period. In both half intervals only two different input current vectors ((ac) and (ab) in the case at hand) are applied and/or two line-to-line input voltages are switched into the DC-link ($u = u_{ac}$ or u_{ab}). Accordingly, the modulation scheme is denoted as „Two-Vector Scheme for Purely Active Load". No volt seconds are added to the output voltage (cf. e.g. u_{BC}) within the second half of the pulse period.
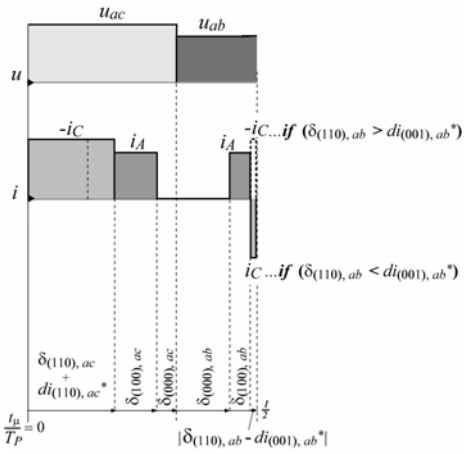

Fig.15: Final pulse pattern resulting for the „Two-Vector-Scheme for purely active load" after merging the output voltage and the input reactive current forming halves of the pulse period depicted in Fig.14.

For Fig.15 we have for the total turn-on time of the active switching states

$$d_{tot,2V,act} = \delta_{(110),ac} + di_{(110),ac}{}^* + \delta_{(100),ac} + $$
$$+ \delta_{(100),ab} + \left| \delta_{(110),ab} - di_{(001),ab}{}^* \right| \qquad (23)$$

For geometrical reasons, (23) is asymmetric in $\varphi_1 = -\pi/6 \dots \pi/6$ and shows a clear minimum in the negative φ_1-half plane. The numerical analysis of (23) yields the operating limit of the *Two-Vector-Scheme* for Purely Active Load depicted in Fig.21 and the critical positions $\varphi_{1,crit}$ within a mains period shown in **Fig.16**.
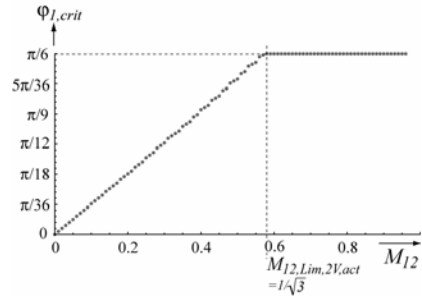

Fig.16 Critical mains phase angle $\varphi_{1,crit,2V,act}$. After the transition to the voltage limiting range ($M_{12} > 1/\sqrt{3}$) the critical mains angle stays constant at $\varphi_{1,crit,2V,act} = \pi/6$.

- **Current Limited Operating Range**
  $\varphi_{2,crit,2V,act} = \pi/6$ (derivation analogous to Section 2.A).
  For $M_{12} \approx 0$: $\varphi_{1crit,2V,act,} = 0$ (like in Section 2.A)
  $MI = \frac{1}{2} \sqrt{3}/2$ (like in Section 2.A).

- **Voltage Limited Operating Range**
  $\varphi_{1,crit,2V,act} = \pi/6$ (like in Section 2.A)
  $\varphi_{2,crit,2V,act} = \pi/6$ (derivation analogous to Section 2.A).

The critical position within the output period is constant
$$\varphi_{2,crit,2V,act} = \pi/6 \qquad (24)$$

An analytical description of the voltage limited operation results in
$$MI_{\max,2V,act}\big|_{M_{12}=1} = \frac{1}{2}\left(1 - \frac{\sqrt{3}}{2}\right) \approx 0.067 \qquad (25)$$
for full modulation.

B. *Three-Vector Modulation Scheme for Purely Active Load*

Considering $\Phi_2 = 0$, again the space vector diagram in Fig.6 is basically valid and yields the additional turn-on times as follows.

$\varphi_1 \geq 0$:
$$di_{(001),ab}{}^* = \frac{2}{\sqrt{3}} MI \cdot \frac{\sin(\varphi_1)}{\cos(\varphi_2)} \qquad (26)$$
$$di_{(110),bc}{}^* = \frac{2}{\sqrt{3}} MI \cdot \frac{\cos(\varphi_1 + \pi/6)}{\cos(\varphi_2)}$$

$\varphi_1 < 0$:
$$di_{(110),ac}{}^* = \frac{2}{\sqrt{3}} MI \cdot \frac{\sin(|\varphi_1|)}{\cos(\varphi_2)} \qquad (27)$$
$$di_{(001),cb}{}^* = \frac{2}{\sqrt{3}} MI \cdot \frac{\cos(|\varphi_1| + \pi/6)}{\cos(\varphi_2)}$$

Fig.17 shows a basic pulse period of the *Three-Vector Scheme for Purely Active Load*. Considering the (partial) pulse compensation, Fig.17 is finally transferred to the pulse pattern depicted in **Fig.18**. It has to be pointed out, that the pulse compensation is not possible for $\varphi_1 < 0$, therefore in this case no reduction of the total turn-on time results, cf. (29).

According to Fig.18 we have

$\varphi_1 \geq 0$:
$$d_{tot,3V,act} = \left| \delta_{(110),ab} - di_{(001),ab}{}^* \right| + \delta_{(100),ab} + \qquad (28)$$
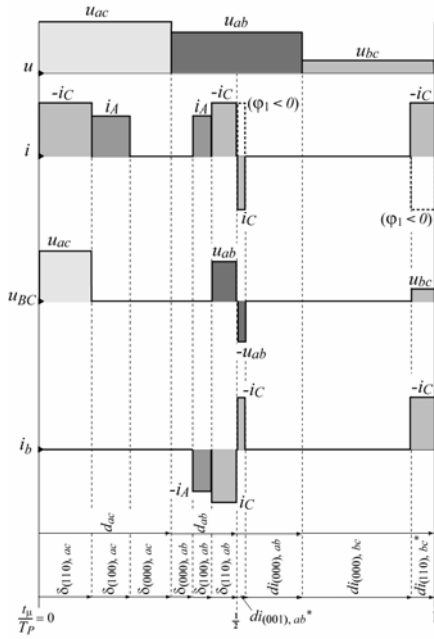$$+ \delta_{(100),ac} + \delta_{(110),ac} + di_{(110),bc}{}^*$$

Fig.17: Hybrid modulation denoted as „Three-Vector Scheme for Purely Active Load". In total three different input current vectors and/or DC-link voltage levels *(ac)*, *(ab)*, *(bc)* are employed within each pulse period. *Remark:* The pulse pattern shown is valid for $\varphi_1 > 0$. In order to point out the main difference in case of $\varphi_1 < 0$ the DC link current pulses are also shown with inverse polarity. Moreover, in this case, the DC link voltage labels u_{ac} and u_{ab} have to be exchanged and u_{bc} has to be replaced by u_{cb} (cf. Fig.18).
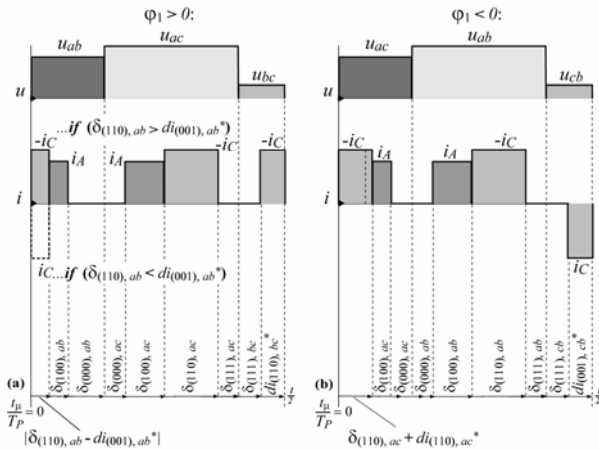

Fig.18: Final pulse pattern resulting for the „Three-Vector Scheme for Purely Active Load ". For $\varphi_1 > 0$ **(a)** input current and/or output voltage pulses occurring for $u=u_{ab}$ in the first and second half of the pulse period depicted in Fig.17 with inverse polarity are partially compensating each other. In contrary, for $\varphi_1 < 0$ **(b)** the pulses occurring for the common DC link voltage level $u=u_{ac}$ show the same polarity. In consequence, no reduction of the total turn-on time can be achieved. *Remark:* Changing the sequence of the voltage pulses forming u as compared to Fig.17 allows to reaching a subsequent level of u by changing only the switching state of either the upper or the lower half of the converter input stage and therefore what minimizes the control complexity.

$\varphi_1 < 0$:

$$d_{tot,3V,act} = \delta_{(110),ac} + di_{(110),ac}{}^* + \delta_{(100),ac} + \\ + \delta_{(100),ab} + \delta_{(110),ab} + di_{(001),cb}{}^* \quad . \tag{29}$$

As for $\varphi_1 < 0$ in principal no turn-on time reduction is possible, $d_{tot,3V,act}$ according to (29) is always lager than the value resulting from (28), a pronounced maximum of $d_{tot,3V,act}$ is located in the

negative φ_1-half plane. This asymmetry is also documented by the dependency of $\varphi_{1,crit,3V}$ shown in **Fig.19**.
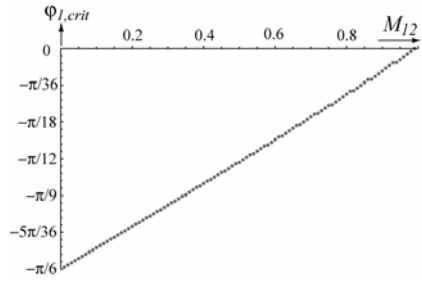

Fig.19: Critical position $\varphi_{1,crit,3V,act}$ within a mains period. As the modulation scheme does not facilitate a reduction of the total turn-on time for $\varphi_1 < 0$ the maximum of $d_{tot,3V,act}$ associated with $\varphi_{1,crit,3V,act}$ is located in the negative φ_1-half plane. In contrary to all other modulation schemes discussed above, the modulation transfers continuously from current to the voltage limited operation.

- **Current Limited Operating Range**
  $\varphi_{2,crit,3V,act} = \pi/6$ (derivation analogous to Section 2.B).
  For $M_{12} \approx 0$: $\quad \varphi_{1,crit,3V,act} = -\pi/6$
  $\qquad\qquad\qquad MI = \frac{3}{4}$ (like in Section 2.B).

- **Voltage Limited Operating Range**
  $\varphi_{1,crit,3V,act} = 0$ (like in Section 2.B)
  $\varphi_{2,crit,3V,act} = \pi/6$ (like in Section 2.B).

The modulation only operates in the current limited range. The critical position within the output period remains constant for changing M_{12} at

$$\varphi_{2,crit,3V,act} = \pi/6 \qquad . \tag{30}$$

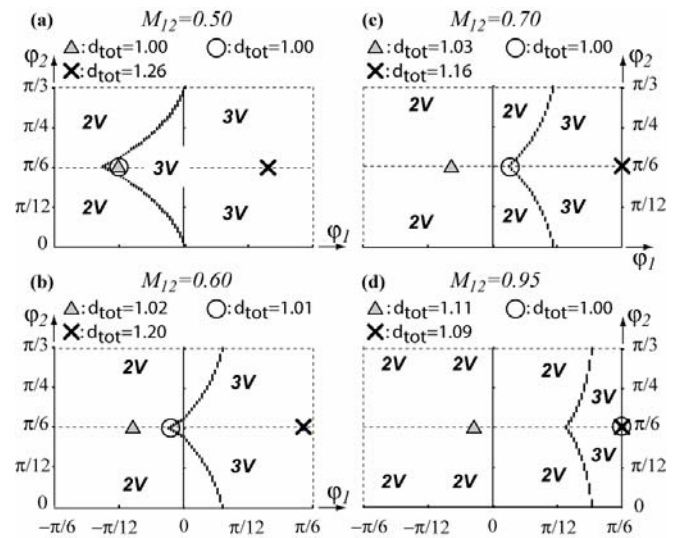### C. Optimum Combination of the Two- and Three-Vector Scheme for Purely Active Load

Fig.20: Domains within the φ_1-φ_2-plane defining the optimum application areas of the *Two-Vector (2V)* or *Three-Vector (3V) Modulation Scheme* with respect to minimum $d_{tot,act}$ (for short also denoted as d_{tot} in the following) for different values of M_{12} and purely active load. In contrast to purely reactive load (cf. Fig.10) the function $d_{tot,opt,act}$ is not symmetric in φ_1 and shows symmetry only concerning φ_2. The *Two-Vector Scheme* is advantageous for negative values φ_1 while the *Three-Vector Scheme* provides allows to achieve minimum values of $d_{tot,act}$ for $\varphi_1 > 0$. Therefore, the location of the boundary separating the application areas is moving for increasing M_{12} from left hand side to the right side. *Legend:* ✗: maximum of $d_{tot,2V,act}$; ▲: max. of $d_{tot,3V,act}$; ○: max. of $d_{tot,opt,act}$.

Due to the asymmetry of both schemes, i.e. the low values of $d_{tot,2V,act}$ occurring for the *Two-Vector Scheme* for $\varphi_I<0$ and the low values of $d_{tot,3V,act}$ given for the *Three-Vector Scheme* for $\varphi_I>0$ the optimum combination allows a larger extension of the operating range as compared to operation with purely reactive load (cf. Section 2.C). This is clearly documented by **Fig.20** and **Fig.21**.

For $M_{12} = 0.50$ **(a)** the global application of the *Three-Vector-Scheme* will not reduce the reactive current component formation capability, since the *Three-Vector-Scheme* still provides the minimum total turn-on time (i.e. $d_{tot,opt,act,max} = d_{tot,3V,act,max}$). With increasing M_{12} (cf. **(b), (c)** in Fig.20) the *Two-Vector-Scheme* has to be employed in the vicinity of the maximum of $d_{tot,3V,act}$ and the *Three-Vector-Scheme* is utilized only in the area containing the maximum of $d_{tot,2V,act}$ what results in an extension of the operating limit as compared to only employing the *Three-Vector Scheme*. When approaching full modulation (cf. **(d)** in Fig.20), the domain of the *Three-Vector-Scheme* still is present resulting in an extended operating range for $M_{12} = 1$ as compared to solely employing the *Two-Vector Scheme*.
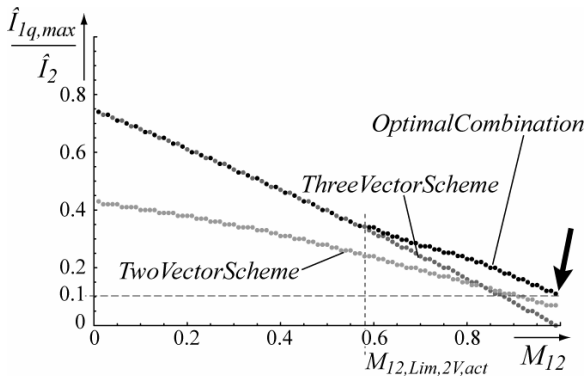

Fig.21: Comparison of the operating limits of the modulation schemes. The optimal modulation is identical to the *Three-Vector Scheme* up to $M_{12,Lim,2V,act}$. From there, the reactive input current formation capability is increased by locally employing the *Two-Vector-Scheme* (cf. Fig.20). For full output voltage ($M_{12} = 1$) the optimal modulation allows to exceed the limit of the *Two-Vector-Scheme* ($MI_{max,opt,act} = 0.1$).

An analytical investigation of the *Two-* and *Three-Vector Scheme* for voltage limited operation confirms the numerically gained value for the operating limit at $M_{12} = 1$ shown in Fig.21

$$MI_{max,opt,act}|_{M_{12}=1} = \tfrac{3}{4}(1-\tfrac{\sqrt{3}}{2}) \approx 0.1005 \qquad . \qquad (31)$$

Taking into account the active input current component given at full output voltage

$$\hat{I}_{1d}|_{M_{12}=1} = \tfrac{\sqrt{3}}{2}\hat{I}_2 \qquad (32)$$

the maximum input current phase displacement angle which could be realized for $\Phi_2=0$ and full output voltage is defined by

$$\Phi_{1,max,opt,act}|_{M_{12}=1} = \pm ArcTan\left[\frac{MI_{max,opt,act}}{\frac{\sqrt{3}}{2}}\right] \approx \pm\frac{\pi}{27}. \qquad (33)$$

This indicates that the theoretical operating limit of the CMC, $\Phi_{1,max,opt,act|M12=1}$=0, specified in [4] for identical operating conditions possibly could be extended by advanced CMC modulation concepts.

IV. DIGITAL SIMULATION AND VERIFICATION

The proposed modulation schemes and the calculated operating limits have been verified by digital simulation using *SIMPLORER* (cf. **Fig.22**).

E.g., for M_{12}=1.0 and MI=0.066 ($\hat{I}_{1q} = MI \cdot \hat{I}_2$, cf. (5)) the amplitude of the reactive component $\bar{i}_{a,reactive}$ of input phase current $\bar{i}_a$ and/or the input current phase displacement (displacement of u_a and $\bar{i}_a$) are showing the expected values ($\Phi_I=-\pi/41$). It should be pointed out that the DC link current i exhibits characteristic negative spikes which are due to the low values of $\delta_{(110),ab}$ in the vicinity of $\varphi_I=\pi/6, \pi/2, 2\pi/3$, etc. as shown in Fig.15.
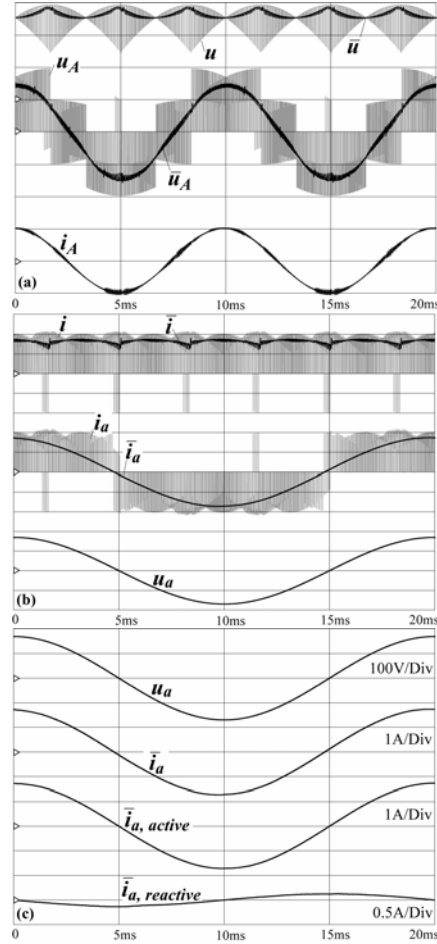

Fig.22: Digital simulation of the operating behavior of the SMC for formation of a reactive input current component at maximum output voltage (M_{12}=1) and purely active load (Φ_2=0); Modulation as shown in Fig.15 with MI=0.066 resulting in an input current phase displacement of $\Phi_I=-\pi/41$; Further parameters: U_I= 170V, f_I=50Hz, f_2=100Hz f_P= 15kHz; L_{Load} =25mH. Scales: **(a)**: 100V/Div, 2A/Div; **(b)**: 100V/Div, 1A/Div. **(c)**: dito, except reactive component: 0.5 A/ Div.

V. CONCLUSIONS

In this paper an optimum combination of the Two- and Three-Vector Modulation of the SMC for maximum utilization of a purely reactive load current for reactive input current generation has been proposed.

Furthermore, it has been shown that the combination of both schemes is applicable also for purely active load, i.e. for Φ_2=0. There, the optimum combination of both schemes significantly extends the SMC operating area in the upper modulation range and facilitates the formation of a reactive input current component and/or a current transfer ratio of $MI \approx 0.1$ even at M_{12} =1 where modulation methods known for the CMC [4] are restricted to MI_{CMC}=0.

Further research will be concentrated on the extension of the optimum modulation schemes to general load conditions i.e. to Φ_2=0...90°. Based on this, the operating limits of the conventional modulation and the Two- and Three-Vector Modulation schems will be compared and the advantageous application areas maximizing the SMC operation range will be clarified.

REFERENCES

[1] **Kolar, J.W., Baumann, M., Schafmeister, F., and Ertl, H.:** *Novel Three-Phase AC-DC-AC Sparse Matrix Converter, Part I and II.*

Proceedings of the 17th Annual IEEE Applied Power Electronics Conference, Dallas (Texas), USA, March 10 - 14, Vol. 2, pp. 777 - 791 (2002).

[2] **Wei, L., and Lipo, T.A.:** *A Novel Matrix Converter Topology with Simple Commutation.* Record of the IEEE Industry Applications Society Annual Meeting, Chicago, Sept. 30 – Oct. 4, Vol. 3, pp. 1749-1754 (2001).

[3] **Schafmeister, F., and Kolar, J.W.:** *Novel Modulation Schemes for Conventional and Sparse Matrix Converters Facilitating Reactive Power Transfer Independent of Active Power Flow.* Proceedings of the 35th Annual IEEE Power Electronics Specialists Conference, Aachen, Germany, June 21-24, pp. 2917-2923 (2004).

[4] **Igney, J., and Braun, M.:** *A New Matrix Converter Modulation Strategy Maximizing the Control Range.* Proceedings of the 35th Annual IEEE Power Electronics Specialists Conference, Aachen, Germany, June 21-24, pp. 2875-2880 (2004).

[5] **Huber, L., and Borojevic, D.:** *Space Vector Modulated Three-Phase to Three-Phase Matrix Converter with Input Power Factor Correction.* IEEE Transactions on Industry Applications, Vol. 31, No. 6, pp. 1234-1246 (1995).

[6] **Kolar, J.W., Schafmeister, F.:** *Novel Modulation Schemes Minimizing the Switching Losses of Sparse Matrix Converters.* Proceedings of the 29th Annual Conference of the IEEE Industry Electronics Society, Roanoke (VA), USA, Nov. 2 - 6, pp. 2085 - 2090 (2003).

[7] **Schafmeister, F., Baumann, M., and Kolar, J.W.:** *Analytically Closed Calculation of the Conduction and Switching Losses of Three-Phase AC-AC Sparse Matrix Converters.* Proceedings of the 10th International Power Electronics and Motion Control Conference, Sept. 9-11, Cavtat & Dubrovnik, Croatia (2002).

[8] **Schafmeister, F., and Kolar, J.W.:** *Verfahren zur Kopplung der ein- und ausgangsseitigen Blindleistungsflüsse dreiphasiger Matrixkonverter.* Patent Application, April 2004.